Charge distribution in thin mesoscopic superconducting rings with enhanced surface superconductivity

Guo-Qiao Zha, Shi-Ping Zhou, Bao-He Zhu, and Yao-Ming Shi
Department of Physics, Shanghai University, 99 Shangda Road, Shanghai 200444, People's Republic of China
(Received 20 November 2005; revised manuscript received 21 December 2005; published 16 March 2006)

The charge distribution in a thin mesoscopic superconducting ring with enhanced surface superconductivity (of a negative surface extrapolation length b) is investigated by the phenomenological Ginzburg-Landau theory. The nature of charge distribution is considerably influenced by the extrapolation length b, the inner and outer radius, and the applied magnetic field. We find a complete negative charge distribution besides the conventional charge distributions of charging vortex states in the Meissner state and the giant vortex state. In addition, one type of charge distribution that only exists in a giant vortex state can also be found in the Meissner state for a ring with a small inner radius. For the multivortex state, we find that the stable multivortex state can exist in small mesoscopic superconducting rings that we studied. The charge distributions for different kinds of multivortex states are given.

DOI: 10.1103/PhysRevB.73.104508 PACS number(s): 74.78.Na, 74.20.De, 74.25.Op, 41.20.Cv

I. INTRODUCTION

The vortex charge in macroscopic type-II superconductors has attracted a lot of attention. In general, it was recognized that spatially inhomogeneous chemical potential can result in a charge distribution, which makes the vortex core charged up.[1,2] In 2000, Kumagai *et al.* first reported the experimental evidence for the presence of the vortex charge by the nuclear magnetic resonance method.[3] Since then, various methods, such as the Ginzburg-Landau (GL) theory,[4] the Bogoliubov-de Gennes model,[5–7] and coupled Bernoulli and Poisson equations[8] were presented to understand the experimental results. Further investigation on this subject was suggested by Yampolskii *et al.*[9] in mesoscopic superconducting disks and cylinders in the framework of the phenomenological Ginzburg-Landau theory. It was shown that, even in the Meissner state, the charge redistribution still exists, which is in contrast to what happened in bulk superconductors, and the charge redistribution is a consequence of the screening currents near the sample edge which makes it behave like a vortex which is turned inside out. A mesoscopic sample is such that its size is comparable to the magnetic field penetration depth λ or the coherence length ξ. Its physical properties are considerably influenced by the size and the geometry of the superconductor. We studied the charge distributions in thin mesoscopic superconducting rings and found that the charge near the inner radius of the ring may change its sign from negative to positive in a giant vortex state with increasing the applied field due to the competition between the paramagnetic Meissner effect and the diamagnetic Meissner effect.[10]

The vortex properties of a mesoscopic superconductor are also strongly influenced by the boundary condition for the order parameter. For a superconductor in contact with a medium with surface enhancement or suppression of superconductivity we have the general boundary condition[11,12]

$$\vec{n}\cdot(-i\vec{\nabla}-\vec{A})\,\psi|_s=\frac{i}{b}\,\psi|_s, \tag{1}$$

where $\vec{n}$ is the unit vector normal to the sample surface, $\vec{A}$ is the vector potential, ψ is the order parameter, and b is the surface extrapolation length which is the effective penetration depth of the order parameter into the surrounding medium. For both the superconductor-vacuum and the superconductor-insulator boundary one has $b\to\infty$, and this case was extensively studied in numerous papers.[9,10,13–23] The case $b>0$ corresponds to surface suppression of the superconducting order parameter, for example, the contact of a superconductor with a normal metal because of the proximity effect. In this case, b is a function of temperature and behaviors of metal and interface.[12,24] The opposite case $b<0$ corresponds to surface enhancement of superconductivity. It can be realized by choosing the suitable material as a surrounding medium, for example, a superconductor having a higher transition temperature than the material of the mesoscopic sample. Another possibility is to use a semiconductor as a surrounding medium, such that there is an overlap of the band gap of the semiconductor with the superconducting gap. The vortex structures of thin mesoscopic disks and cylinders allowing for the enhanced surface superconductivity were studied in Refs. 25 and 26, respectively. The authors found that increasing the superconductivity near the surface leads to higher critical fields and critical temperatures, and the surface enhancement of superconductivity can stabilize the multivortex state.

In the present paper we investigate the vortex structure and the charge redistribution around vortices of thin mesoscopic rings in a perpendicular magnetic field surrounded by a medium with enhanced surface superconductivity. The ring has more than one boundary in comparison with a disk sample and its vortex properties can be strongly influenced by the surface enhancement of superconductivity. More complex and interesting features are expected. We extend the approach in our previous studies[10] and present a systematic study of the charge distribution. We find that the surface enhancement of superconductivity can increase the negative charge of the sample and a complete negative charge distribution will present for the Meissner state and the giant vortex state besides conventional distributions of charging vortex states. In addition, in the Meissner state one type charge

distribution, that can only be found in giant vortex state, can also exist in a ring with a small inner radius. These charge distributions are considerably influenced by the surface extrapolation length b, the inner radius R_i and the outer radius R_o, and the applied magnetic field strength as well. It is also found that the surface enhancement of superconductivity can stabilize the multivortex state, and the stable multivortex state can exist in small rings that we studied. The charge distributions for the saddle-point state and the stable multivortex state are given finally.

The paper is organized as follows. In Sec. II we present our theoretical model and give the necessary formalism. Computations are performed as the ring size and magnetic field vary. The charge distributions in both the Meissner state and the giant vortex states are presented in Sec. III, whereas those in the multivortex states are discussed in Sec. IV, and some conclusive remarks and discussions are given in Sec. V.

II. THEORETICAL APPROACH

We consider mesoscopic superconducting rings with outer radius R_o and inner radius R_i and thickness d surrounded by a medium which enhances superconductivity at the sample surface. We restrict ourselves to sufficiently thin rings such that $d \ll \xi, \lambda$. In this case, the external magnetic field $\vec{H}$ is uniform and directed normal to the rings plane. The Cooper pair density $|\psi(\vec{r})|^2$ is determined from a solution of coupled nonlinear GL equations for the superconducting order parameter $\psi(\vec{r})$ and the magnetic field $\vec{h}(\vec{r}) = \vec{\nabla} \times \vec{A}(\vec{r})$,

$$(-i\vec{\nabla} - \vec{A})^2 \psi = \psi - \psi|\psi|^2, \tag{2}$$

$$\kappa^2 \vec{\nabla} \times \vec{\nabla} \times \vec{A} = \vec{j}, \tag{3}$$

where the density of the superconducting current $\vec{j}$ given by

$$\vec{j} = \frac{1}{2i}(\psi^* \vec{\nabla} \psi - \psi \vec{\nabla} \psi^*) - |\psi|^2 \vec{A}. \tag{4}$$

We use the cylindrical coordinates $\vec{r} = (\rho, \theta, z)$ and choose the gauge $\vec{A} = (H\rho/2)\vec{e}_\theta$. ρ is the radial distance from the ring center, θ is the azimuthal angle, and the z axis is taken perpendicular to the ring plane, and the ring lies between $z = d/2$ and $z = -d/2$. We measure the distance in units of the coherence length $\xi = \hbar/\sqrt{2m|\alpha|}$, and the vector potential in $c\hbar/2e\xi$, the magnetic field in $H_{c2} = c\hbar/2e\xi^2 = \kappa\sqrt{2}H_c$, and the superconducting current in $j_0 = cH_c/2\pi\xi$. Where H_c is the thermodynamical critical field, and $\kappa = \lambda/\xi$ is the GL parameter.

In a type-II superconductor ($\kappa > 1/\sqrt{2}$), the "*vortex free*" Meissner state becomes energetically unfavorable in comparison with a triangle vortex lattice state when the magnetic field $H > H_{c1}$. Khomskii and Freimuth showed that the vortex core should be charged up due to the chemical potential in the superconducting state breaking the particle-hole symmetry which is different from that in the vortex core (normal region).[1] However, the charge accumulated in the core is determined by the magnitude of $(\Delta/\epsilon_F)^2$, where Δ is the energy gap and ϵ_F the Fermi level, which is small for metallic superconductors. On the other hand, Hayashi *et al.* suggested that vortices were intrinsically charged up in superconductors having a small value of $k_F\xi$, that is, a fast variation of wave function.[7] Koláček *et al.* showed that an

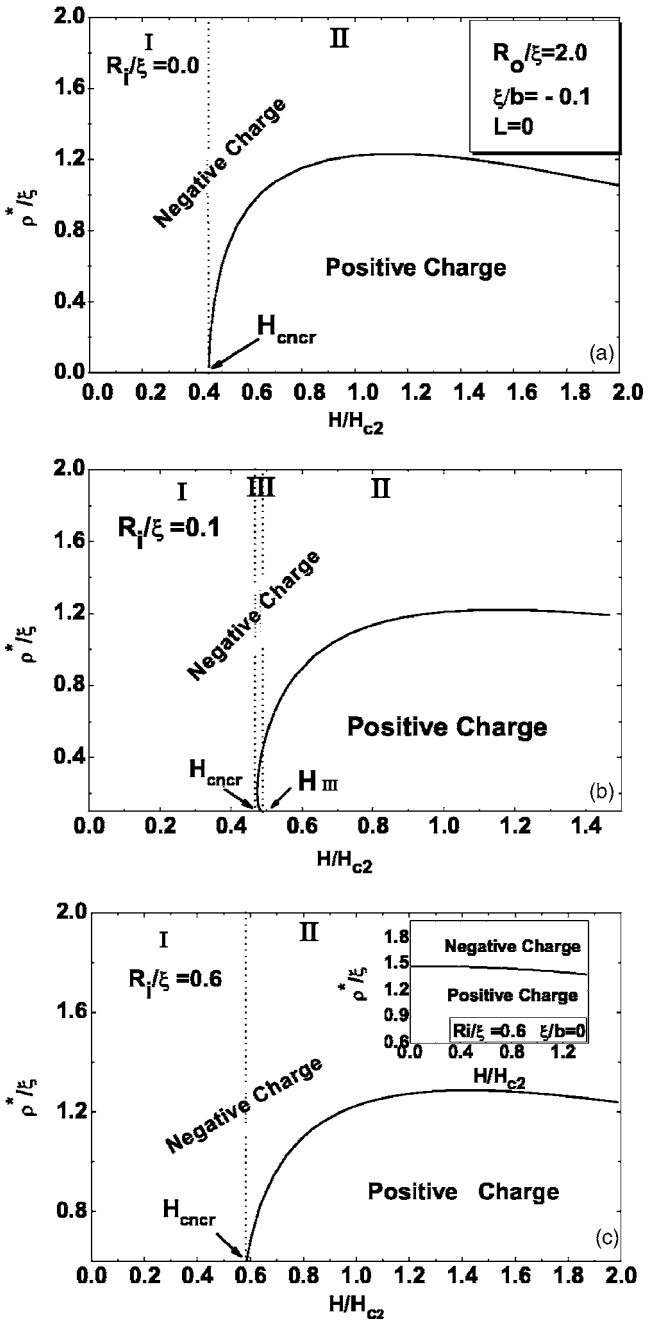

FIG. 1. The applied magnetic field H dependence of the radius ρ^* for superconducting rings with outer radius $R_0/\xi = 2.0$, $\xi/b = -0.1$, $d/\xi = 0.1$ and inner radius $R_i/\xi = 0.0$ (a), $R_i/\xi = 0.1$ (b), $R_i/\xi = 0.6$ (c) in the Meissner state. H_{cncr} denotes the critical magnetic field, where the complete negative charge region (i.e., the region **I**) disappears and $H_{\mathbf{III}}$ denotes the critical magnetic field where the region **III** disappears. The inset in (c) is for a superconducting ring with outer radius $R_0/\xi = 2.0$, inner radius $R_i/\xi = 0.6$, and $\xi/b = 0$.

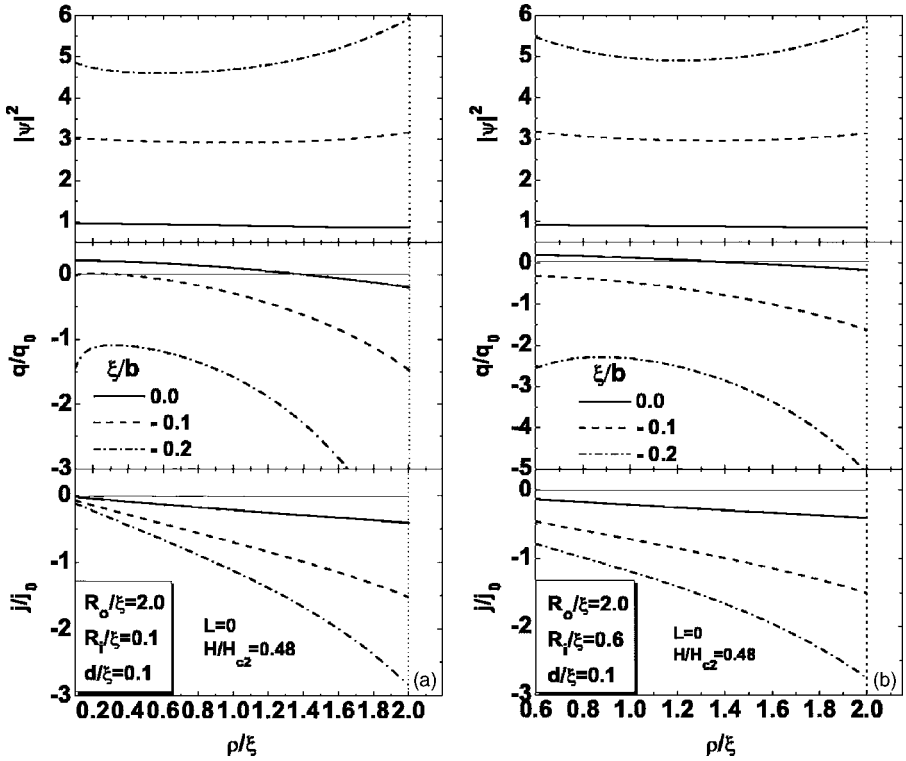

FIG. 2. The radial dependence of the Cooper pair density $|\psi(\rho)|^2$, the charge density $q(\rho)$, and the supercurrent density $j(\rho)$ when $H=0.48H_{c2}$ and different b values in $L=0$ state for rings with outer radius $R_0/\xi=2.0$ and inner radius $R_i/\xi=0.1$ (a), $R_i/\xi=0.6$ (b).

electrostatic potential φ is induced by the inhomogeneous order parameter via[27]

$$\varphi(\vec{\rho}) = \varphi_0(|\psi(\vec{\rho})|^2 - 1), \tag{5}$$

where $\varphi_0=|\alpha|/2e$. The distribution of the charge density $q(\vec{\rho})$ is obtained from the Poisson equation

$$4\pi q(\vec{\rho}) = -\nabla^2\varphi(\vec{\rho}). \tag{6}$$

Using the Gauss theorem as well as the boundary condition (1) and its complex conjugate, the total charge Q is given by:

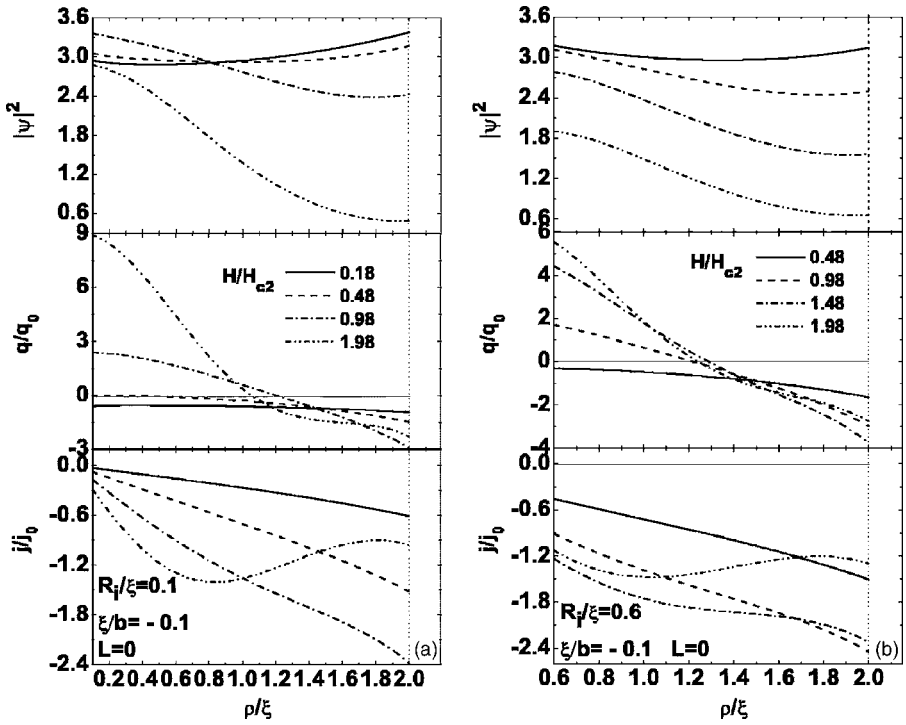

FIG. 3. The radial dependence of the Cooper pair density $|\psi(\rho)|^2$, the charge density $q(\rho)$ and the supercurrent density $j(\rho)$ when $\xi/b=-0.1$ and different magnetic fields in $L=0$ state for rings with outer radius $R_0/\xi=2.0$ and inner radius $R_i/\xi=0.1$ (a), $R_i/\xi=0.6$ (b).

$$Q \equiv -\frac{|\alpha|}{8\pi e}\int_v \nabla^2|\psi(\vec{r})|^2 dV = \frac{|\alpha|}{4\pi e b}\int_S |\psi(\vec{r})|^2 dS. \quad (7)$$

So the sample should have a finite total charge whose sign is determined by the sign of b.

Note added: There exists the surface charge[28] on the scale of the Thomas-Fermi screening length due to the charge screening effect, which then would influence the profile of the charge induced by the superconducting state,[29] e.g., the Friedel oscillation in a charge profile,[6] and the sign of the total charge remains unchanged.[6] Strictly speaking, the surface charge due to the charge screening effect would contribute somewhat a net charge to the total charge for a finite extrapolation length $1/b$ of nonzero. But, it will, in general, not change the sign of the total (net) vortex charge, since the charge distribution oscillates about the "*body*" charge level over approximately the distance scale of the Thomas-Fermi screening length.[6,29] On the other hand, when the extrapolation length $1/b$ tends to zero, the total surface charge, as the total body charge, must be zero for the electric neutrality of the sample.

The free energy of the superconducting state is determined by the expression

$$F = \frac{2}{V}\Bigg[\int dV\Bigg(-|\psi|^2 + \frac{1}{2}|\psi|^4 + |-i\vec{\nabla}\psi - \vec{A}\psi|^2 + \kappa^2[\vec{h}(\vec{r}) - \vec{H}]^2\Bigg) + \frac{1}{b}\oint dS|\psi|^2\Bigg]. \quad (8)$$

The last term in Eq. (8) is the surface contribution and it provides continuity of the normal component of the superconducting current. One can see that in the $b<0$ case this term reduces the free energy, implying the superconductivity enhanced effect.

We assume $\psi(\vec{\rho},z)=\Sigma_k\psi_k(\vec{\rho})[A\exp(ikz)+B\exp(-ikz)]$, where A and B are constants, and the wave number (or the quantum number of z direction) k is determined from the boundary condition (1) at $z=d/2$, and $-d/2$. For the symmetry of the z axis, we choose $A=B$, resulting in

$$kb = i\frac{\exp(ikd/2)+\exp(-ikd/2)}{\exp(ikd/2)-\exp(-ikd/2)} = \frac{\cos(kd/2)}{\sin(kd/2)}. \quad (9)$$

For a thin sample, that is $d\to 0$, the lowest k is given by:

$$k^2 = \frac{2}{bd}, \quad (10)$$

which is negative when $b<0$ (the surface superconductivity enhanced case). Denote $k=i\Gamma$ with $\Gamma^2=-2/bd>0$, the wave function reduces to: $\psi(\vec{\rho},z)=\psi(\vec{\rho})\cosh(\Gamma z)$.

Since ψ varies very slowly along the z direction for $|d/b|\ll 1$, we can average the order parameter over the disk thickness:

$$\langle\psi(\vec{r})\rangle = \frac{1}{d}\int_{d/2}^{-d/2}\psi(\vec{\rho})\cosh(\Gamma z)dz = \psi(\vec{\rho})\cdot\frac{\sinh(\Gamma d/2)}{\Gamma d/2} \to \psi(\vec{\rho}). \quad (11)$$

The same averaging of Eq. (2) yields for $\psi(\vec{\rho})$:

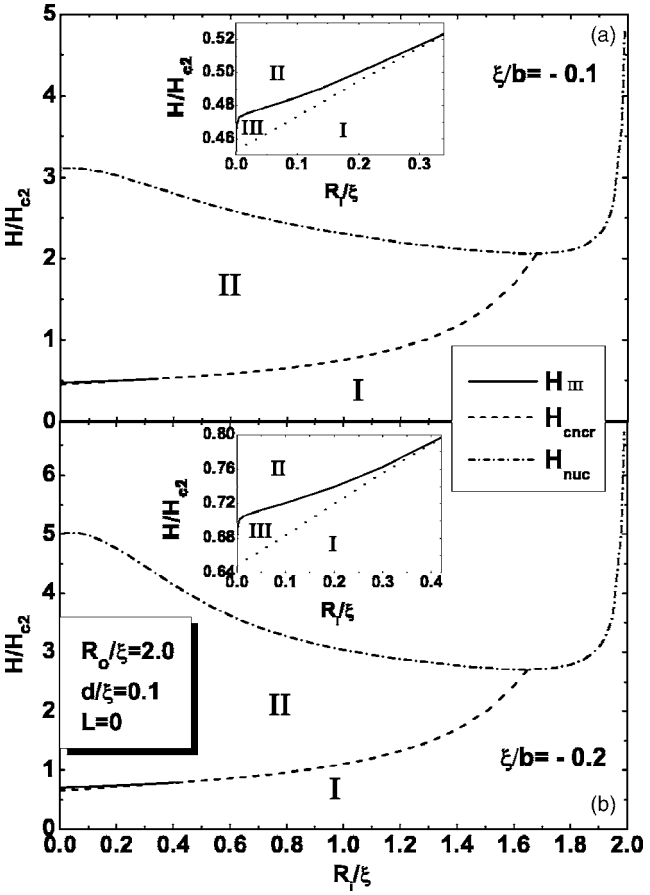

FIG. 4. The phase diagrams $H-R_i$ for the superconducting rings with outer radius $R_0/\xi=2.0$, $d/\xi=0.1$ and $\xi/b=-0.1$ (a), $\xi/b=-0.2$ (b) in the $L=0$ state. The insets are an enlargement of the region **III**. The H_{nuc} denotes the nucleation field.

$$\langle(-i\vec{\nabla}-\vec{A})^2\rangle\psi(\vec{\rho}) = \Bigg[-\frac{1}{\rho}\frac{\partial}{\partial\rho}\rho\frac{\partial}{\partial\rho} - \frac{1}{\rho^2}\frac{\partial^2}{\partial\theta^2} + iH\frac{\partial}{\partial\theta} + \left(\frac{H\rho}{2}\right)^2 - \Gamma^2\Bigg]\psi(\vec{\rho}) = \psi(\vec{\rho}) - \psi(\vec{\rho})|\psi(\vec{\rho})|^2. \quad (12)$$

Now the boundary condition is given by

$$\left.\frac{\partial\psi(\vec{\rho})}{\partial\rho}\right|_{\rho=R_i} = \left.\frac{1}{b}\psi(\vec{\rho})\right|_{\rho=R_i}, \qquad \left.\frac{\partial\psi(\vec{\rho})}{\partial\rho}\right|_{\rho=R_o} = -\left.\frac{1}{b}\psi(\vec{\rho})\right|_{\rho=R_o}. \quad (13)$$

III. CHARGES IN THE MEISSNER AND THE GIANT VORTEX STATES

The giant vortex state has cylindrical symmetry and consequently the order parameter can be written as $\psi(\vec{\rho})=f(\rho)\exp(iL\theta)$. Define

$$\hat{L} = -\frac{1}{\rho}\frac{\partial}{\partial\rho}\rho\frac{\partial}{\partial\rho} + \left(\frac{L}{\rho}-\frac{H\rho}{2}\right)^2 - 1 - \Gamma^2, \quad (14)$$

and

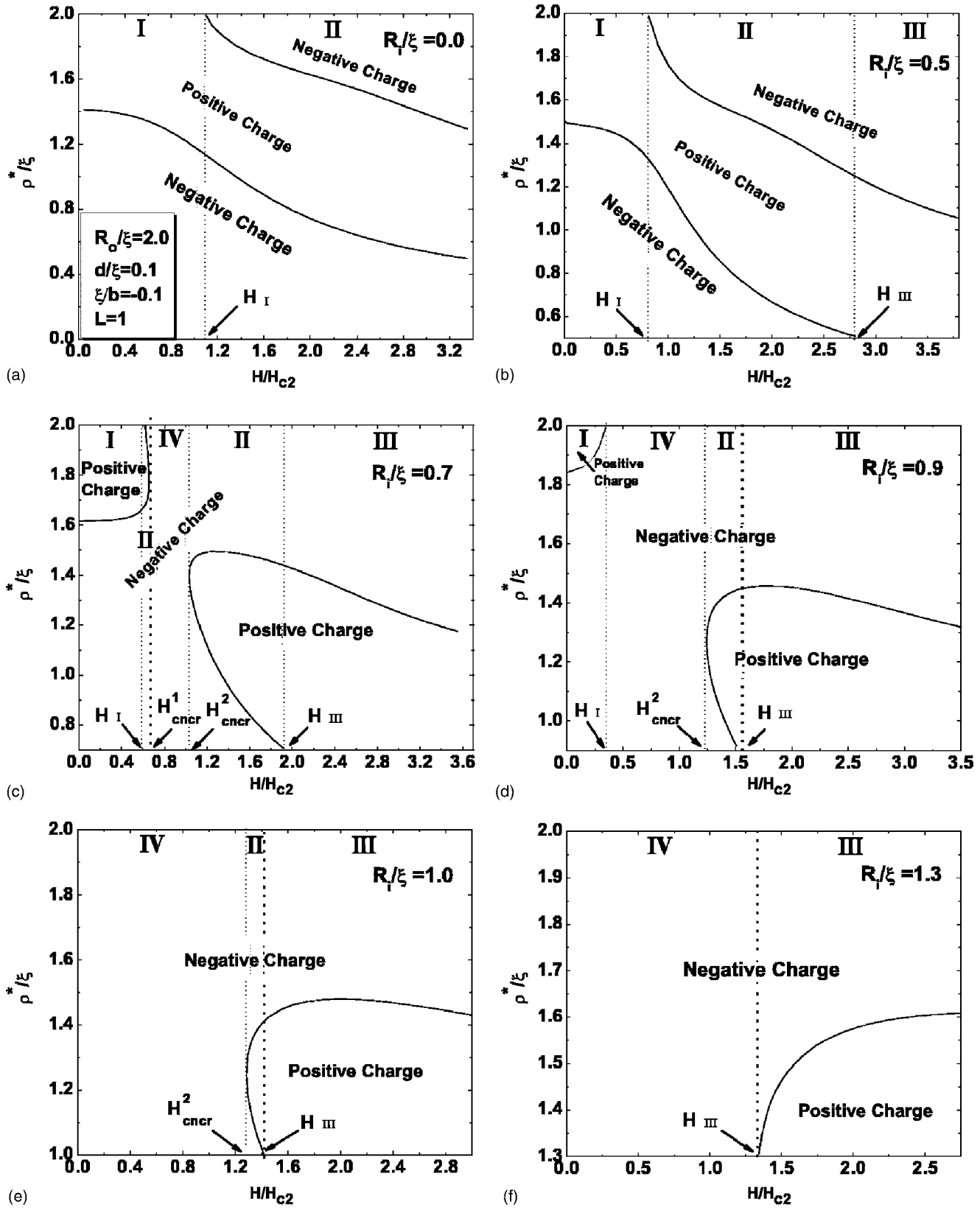

FIG. 5. The applied magnetic field H-dependence of the radius $\rho*$ for superconducting rings with different inner radius R_i in the $L=1$ state. We choose $R_0/\xi=2.0$, $\xi/b=-0.1$, and $d/\xi=0.1$. $H_{\mathbf{I}}$ and $H_{\mathbf{III}}$ denote the magnetic fields where the sign reversal for the inner charge and the outer charge occur, respectively. H^1_{cncr} and H^2_{cncr} denote the critical magnetic fields where the CNCR occurs and disappears, respectively.

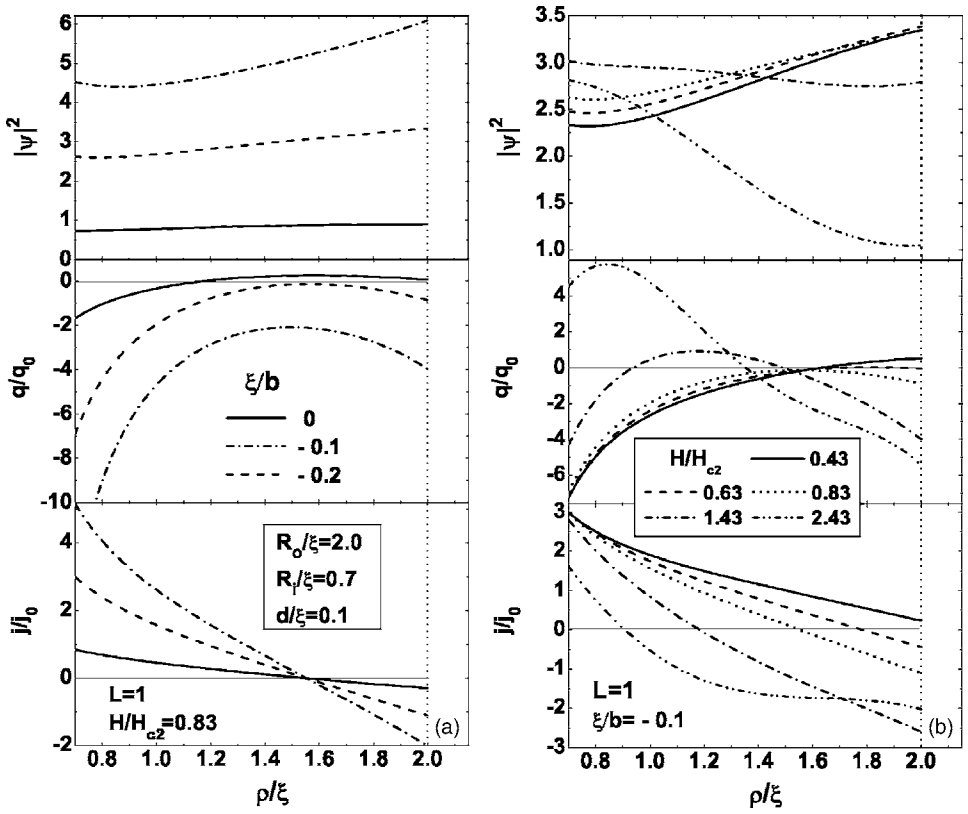

FIG. 6. The radial dependence of the Cooper pair density $|\psi(\rho)|^2$, the charge density $q(\rho)$ and the supercurrent density $j(\rho)$ for a ring with outer radius $R_0/\xi=2.0$, inner radius $R_i/\xi=0.7$ in $L=1$ state when in (a) fixed magnetic fields but different b values, (b) fixed b value but different magnetic fields.

$$\hat{L} f_{L,n}(\rho) = \Lambda f_{L,n}(\rho). \tag{15}$$

Let $x=H\rho^2/2$, and $f_{L,n}(x)=x^{L/2}e^{-x/2}g(x)$. We can prove that $g(x)$ can be any linear combination of the two confluent hypergeometric functions (or first and second types of Kummer functions) $M(a,c,x)$ and $U(a,c,x)$. Then

$$f_{L,n}(\rho) = \left(\frac{H\rho^2}{2}\right)^{L/2} \exp\left(-\frac{H\rho^2}{4}\right) \times \left[AM\left(-\upsilon_n, L+1, \frac{H\rho^2}{2}\right) + BU\left(-\upsilon_n, L+1, \frac{H\rho^2}{2}\right)\right], \tag{16}$$

where υ_n and constants A and B have to be solved numerically from the boundary condition (13), and the number n enumerates the states for the same L value. The eigenvalues of $\hat{L}$ are

$$\Lambda = (1+2\upsilon_n)H - 1 - \Gamma^2. \tag{17}$$

The order parameter then is expressed as

$$\psi(\vec{\rho}) = C f_{L,n}(\rho)\exp(iL\theta), \tag{18}$$

and a right multiple constant C will then lead to a minimum free energy:

$$F = -\Lambda^2 \frac{2\pi d}{V}\frac{I_2^2}{I_1}, \tag{19}$$

where $I_1=\int_{R_i}^{R_o}\rho d\rho f_{L,n}^4(\rho)$, $I_2=\int_{R_i}^{R_o}\rho d\rho f_{L,n}^2(\rho)$, and the free energy is measured in units of $F_0=H_c^2V/8\pi$.

A. Meissner state

First, we study the $L=0$ state, i.e., the Meissner state. We consider superconducting rings with the outer radius $R_o=2.0\xi$ surrounded by a medium with $\xi/b=-0.1$. All numerical calculations are done for a thickness $d/\xi=0.1$, whereas $|\xi/b|<0.5$, which are then within the thin ring approximation. The charge density is measured in units of $q_0=\hbar^2/32\pi me\xi^4$. Define $\rho*$ a distance from the ring center where the sign reversal of the vortex charge occurs. Figure 1 plots the phase diagrams of H versus $\rho*$ for positive and negative charge distributions for these rings with $R_i=0.0\xi$ (a), $R_i=0.1\xi$ (b), and $R_i=0.6\xi$ (c). The inset in Fig. 1(c) is for $\xi/b=0$, i.e., without the enhanced surface superconductivity effect. From Fig. 1 we can find that for small field there is a complete negative charge distribution (i.e., the region **I**), that is, the sample is completely negatively charged. However, it will neither occur in a ring without the enhanced surface superconductivity [see the inset in Fig. 1(c)] nor in a disk immersed in an insulating medium.[9] Interestingly, as the applied magnetic field is increased to the critical field H_{cncr}, the complete negative charge region (i.e., the region **I**) disappears and the region **III**, where the signs of the charge near the inner boundary and the outer boundary are both negative while the rest region is positive, will occur in a fat ring [Fig. 1(b)]. This charge distribution can only be found in the giant vortex state before.[9,10] Further increasing the magnetic field, the region **III** disappears at the critical field $H_{\mathbf{III}}$ and the charge near the inner boundary changes to positive, while the charge near the outer boundary still is negative (i.e., the region **II**). We notice that there is no region **III** in Figs. 1(a) and 1(c) and the region **I** changes to the region **II** directly with increasing the field.

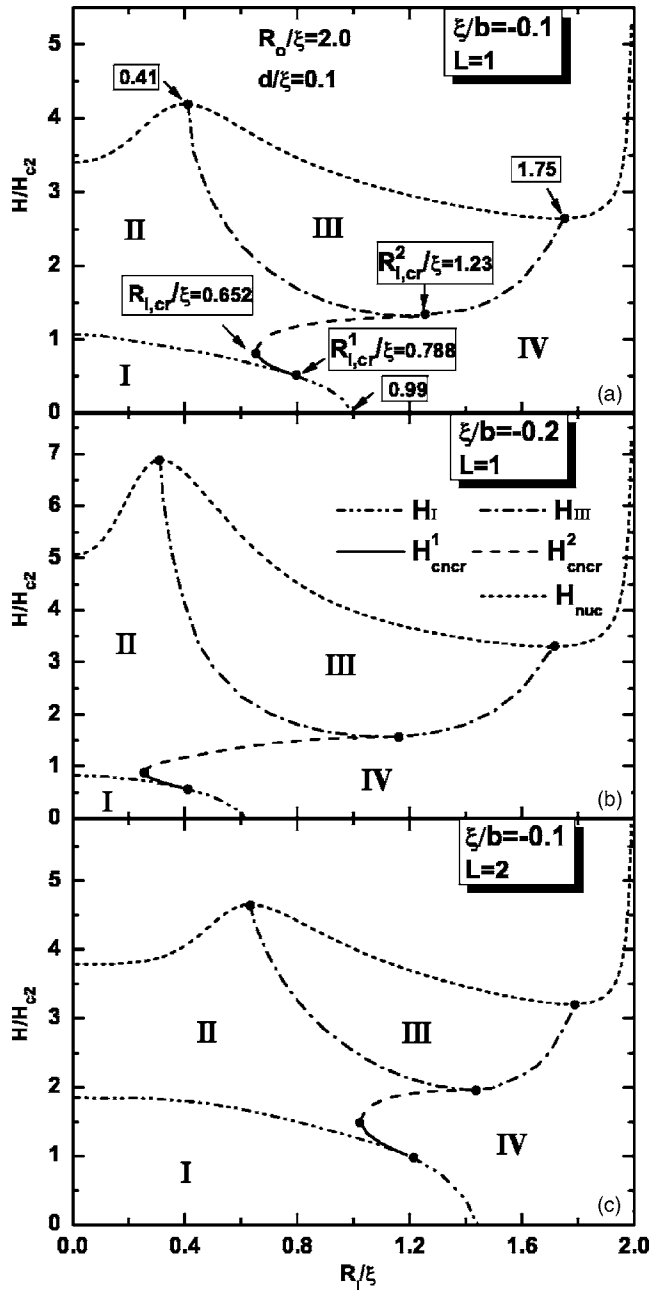

FIG. 7. The phase diagrams of R_i versus $H_{\mathbf{I}}$, $H_{\mathbf{III}}$, H_{nuc}, and H_{cncr} for superconducting rings with $R_0/\xi=2.0$, $d/\xi=0.1$, and (a) $\xi/b=-0.1$, $L=1$, (b) $\xi/b=-0.2$, $L=1$, (c) $\xi/b=-0.1$, $L=2$. H_{nuc} denotes the nucleation field. The solid circles denote the critical inner radii when the regions of different charge distributions occur or disappear.

These different charge redistributions can be explained as follows. Figure 2 gives the radial dependence of the Cooper pair density $|\psi(\rho)|^2$, the charge density $q(\rho)$, and the supercurrent density $j(\rho)$ when $H=0.48H_{c2}$ in $L=0$ state corresponding to the rings in Figs. 1(b) and 1(c) with different b values. Due to the finite radial size of the sample, all distributions are inhomogeneous along the radius of the sample. In $L=0$ state, the superconductor expels the magnetic field by inducing a supercurrent, which tries to compensate the applied magnetic field in the superconductor and inside the hole. When there presents no enhanced surface superconductivity effect, the Cooper pair density is maximum at the inner boundary and decays towards the outer boundary. So there is a region of positive charge near the inner boundary and the negative "*screening*" charge is created near the outer boundary. Due to the enhanced surface superconductivity, we find that the Cooper pair density in whole sample increases, but inside the sample the Cooper pair density is not increasing as strong as the Cooper pair density near the boundary. Enhancing the surface superconductivity results in a stronger Meissner effect, i.e., the magnetic field expulsion becomes more complete with increasing $|\xi/b|$. So the superconductor has to induce more supercurrent to expel the magnetic field. From Fig. 2 we get that the current densities in the two samples both become more negative and the current density near the outer boundary increases more quickly than the inner boundary. As a result, the negative charge near the outer boundary increases and is pulled towards the inner boundary with increasing $|\xi/b|$. So the complete negative charge region (CNCR) occurs. For a ring with fixed b value but different magnetic fields, Fig. 3 gives the radial dependence of the Cooper pair density $|\psi(\rho)|^2$, the charge density $q(\rho)$, and the supercurrent density $j(\rho)$ corresponding to the rings in Figs. 1(b) and 1(c). Because of the enhanced surface superconductivity, they are both in the CNCR at small field. Increasing the magnetic field the induced supercurrent becomes more negative and leads to a depression of the Cooper pair density. So the negative charge near the inner boundary decreases while the negative charge near the outer boundary increases with increasing the field. For a ring with small inner radius, the Cooper pair density near the outer boundary decreases with increasing the magnetic field, while near the inner boundary the Cooper pair density increases initially [Fig. 3(a)], i.e., the magnetic field inside the hole is considerably suppressed due to the the enhanced surface superconductivity. As a result, the negative charge at the inner boundary decreases slowly and then the region **III** will occur. Further

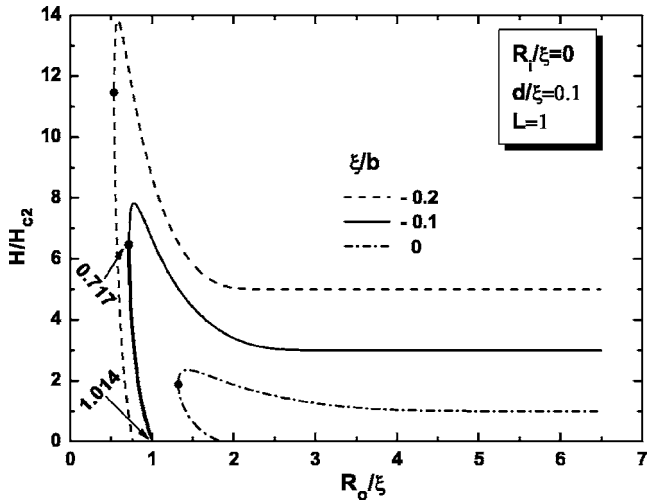

FIG. 8. The nucleation field H_{nuc} as a function of the outer radius of rings with $R_i/\xi=0$ and different ξ/b for the $L=1$ state. The thin solid curve denotes the upper nucleation field and the thick solid curve denotes the lower nucleation field.

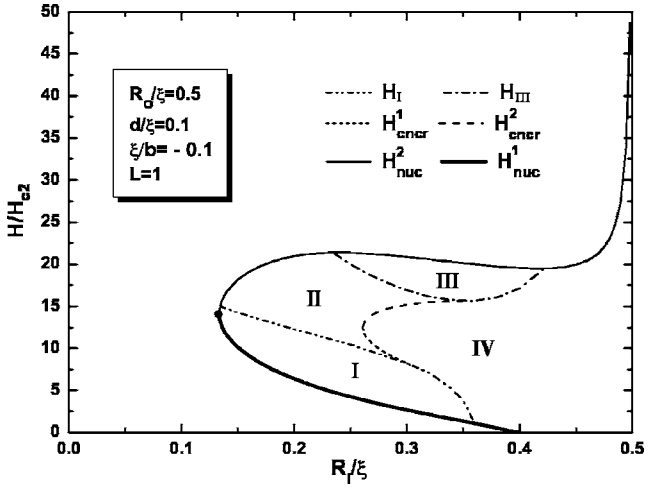

FIG. 9. The phase diagram of R_i versus $H_{\mathbf{I}}$, $H_{\mathbf{III}}$, H_{nuc}, and H_{cncr} for superconducting rings with $R_0/\xi=0.5$, $d/\xi=0.1$, and $\xi/b=-0.1$ in the $L=1$ state. H^1_{nuc} denotes the lower nucleation field (thick solid curve) and H^2_{nuc} denotes the upper nucleation field (thin solid curve). The solid circle denotes the critical inner radius when the superconducting state can occur.

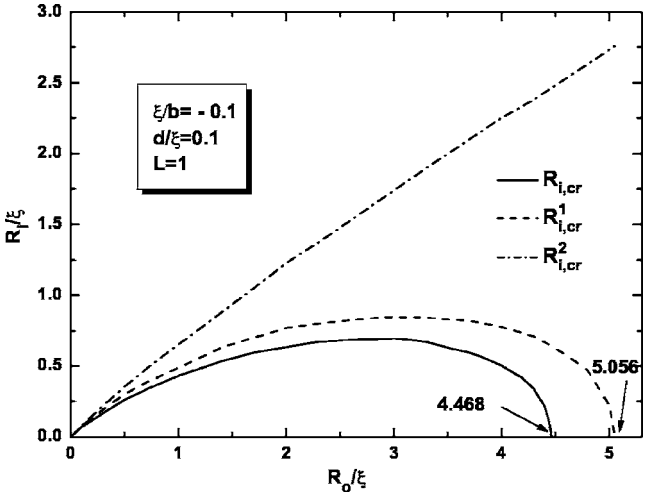

FIG. 10. The transition inner radii $R_{i,cr}$, $R^1_{i,cr}$, and $R^2_{i,cr}$ dependence of the outer radius R_o for superconducting rings with $\xi/b=-0.1$ and $d/\xi=0.1$ in the $L=1$ state.

increasing the field, the charge near the inner boundary will become a positive charge completely, but the sign of the charge near the outer boundary remains (i.e., the region **II** will occur).

Figure 4 shows the phase diagram of R_i versus the critical magnetic fields H_{cncr}, $H_{\mathbf{III}}$ and the nucleation field H_{nuc} for superconducting rings with an outer radius $R_0/\xi=2.0$ and $\xi/b=-0.1$ (a), $\xi/b=-0.2$ (b) in the $L=0$ state. The H_{nuc} is the critical field for the transition between the superconducting state and the normal state. The insets are an enlargement of the region **III**. We find that the critical field H_{cncr} becomes larger with increasing $|\xi/b|$ and changes quickly for a large inner radius. The region **III** is very small and can only exist in rings with a small inner radius. When the inner radius becomes very large, the region **II** also disappears, that is to say, the ring is negatively charged as long as it is in the superconducting state. In addition, the nucleation field H_{nuc} becomes very large when $R_i \approx R_0$, which is a consequence of the enhancement of surface conductivity for very small samples.

B. Giant vortex state

Now, we investigate the giant vortex state. Figure 5 plots the applied magnetic field H-dependence of the radius ρ^* for different superconducting rings with the same outer radius $R_0/\xi=2.0$ and $\xi/b=-0.1$ in the $L=1$ state. The charge distributions become more complicated in comparison with those shown in Fig. 1 for $L=0$ state. In Fig. 5(a) for a ring with an inner radius $R_i/\xi=0$, i.e., a disk, there are only two regions: (i) the region **I**, where the charge near the inner boundary is negative and the charge near the outer boundary is positive, and (ii) the region **II**, where the charge near the inner boundary and the outer boundary are both negative and the inside is positive. With increasing inner radius R_i, the region **III**, i.e., the charge near the inner boundary is positive and the charge near the outer boundary is negative, appears [see Fig. 5(b)]. The same charge distribution can be found in Ref. 10, but because of the enhanced surface superconductivity we only need a smaller inner radius. Interestingly, we find that the complete negative charge distribution (i.e., the region **IV**) also can occur in the $L=1$ state, and the region **I** and the region **II** decrease and disappear finally with increasing the inner radius from (c) to (f). In Fig. 5(f) there are only the CNCR and the region **III** as happened for the $L=0$ state.

Figure 6 gives the radial dependence of the Cooper pair density $|\psi(\rho)|^2$, the charge density $q(\rho)$, and the supercurrent density $j(\rho)$ in $L=1$ state for the ring in Fig. 5(c). Figure 6(a) shows the case for a fixed magnetic field but different b values. We find that negative charge increases in the whole sample due to the enhanced surface superconductivity and the complete negative charge region occurs. With increasing $|\xi/b|$ the negative charge in the whole sample increases. Figure 6(b) is the case for fixed b but different magnetic fields. We can get that at a small field where there is a minimum of the Cooper pair density near the inner boundary because more flux is trapped in the hole in the $L=1$ state and the local magnetic field inside the hole becomes larger than the external magnetic field. So the sample near the inner boundary and the outer boundary are negatively and positively charged, respectively (i.e., the region **I**). Notice that the sign of the induced current is positive in the whole superconductor at the small field, that is to say, the magnetic field is only expelled to the hole. With increasing the magnetic field the sign of the current near the outer boundary changes to negative, i.e., the magnetic field is expelled not only to the outside of the system but also to the hole. So the sign of the charge near the outer boundary will become negative, i.e., the region **II** occurs. If the inner radius of a ring is big enough, the enhanced surface superconductivity effect will influence not only the boundary but also the inside of the sample. Then the sign of the charge in the whole sample will become negative with increasing the field because of this effect (i.e., the CNCR). Further increasing the field, the Cooper pair density near the inner boundary increases and be-

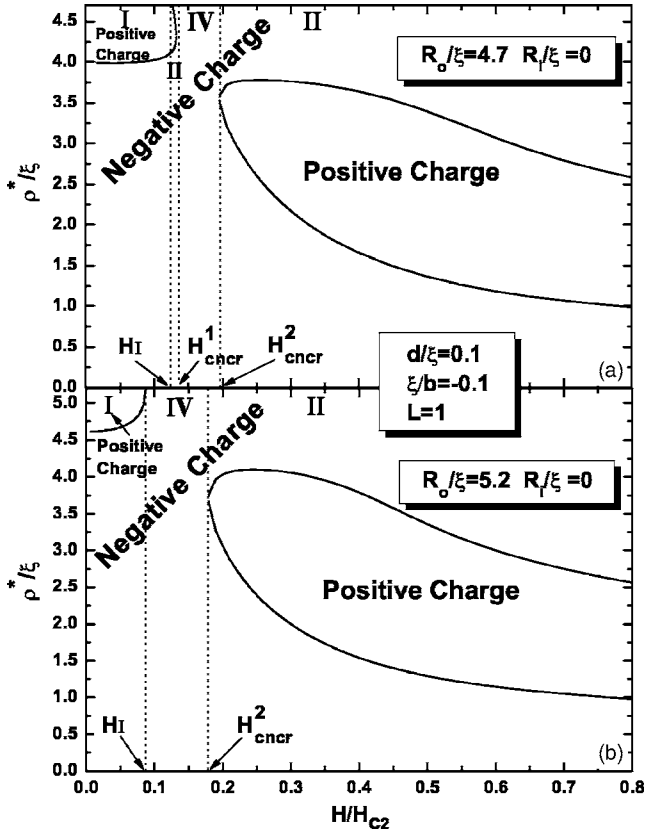

FIG. 11. The applied magnetic field H-dependence of the radius $\rho*$ for two superconducting disks $R_o/\xi=4.7$ (a), $R_o/\xi=5.2$ (b) with $\xi/b=-0.1$ and $d/\xi=0.1$ in the $L=1$ state.

comes larger than the Cooper pair density near the outer boundary. The current density near the inner boundary becomes less positive. So the negative charge near the inner boundary decreases and then the sign becomes positive. In this case, we find that the positive charge is pulled towards the inner boundary with increasing the magnetic field, but the region of the positive charge expands. In addition, the enhanced surface superconductivity effect for a very narrow ring becomes stronger in whole sample comparing with a fat ring. So the regions **I** and **II** will disappear [Figs. 5(d)–5(f)].

Figure 7(a) plots the phase diagram, that is the boundaries that separate different types of charge distribution $H_{\mathbf{I}}$, $H_{\mathbf{III}}$, H_{nuc}, and H_{cncr} as the inner radius R_i varies. From Fig. 7(a), we find that the region **III** does not exist if $R_i<0.41\xi$, which is analogous to a disk case. When $R_i/\xi=0.41$, the magnetic field $H=H_{\mathbf{III}}=H_{nuc}$. Increasing R_i from 0.41ξ slowly, the region **III** occurs, while the region **II** and the region **I** are getting less. Then when $R_i=R_{i,cr}=0.652\xi$, the CNCR occurs, and the region **II** is separated into two parts (where the $R_{i,cr}$ denotes the critical inner radius when the CNCR occurs). We notice that the region **II** in a high magnetic field is larger than the region **II** in a low magnetic field, i.e., the region **I** changes to the CNCR directly when $R_i>R^1_{i,cr}=0.788\xi$ and the CNCR changes to the region **III** directly when $R_i>R^2_{i,cr}=1.23\xi$ (where the $R^1_{i,cr}$ and $R^2_{i,cr}$ denote the critical inner radii when the region **II** is at low magnetic field and at high magnetic field disappears, respectively). When $R_i=0.99\xi$, the region **I** disappears, and when $R_i=1.23\xi$, only

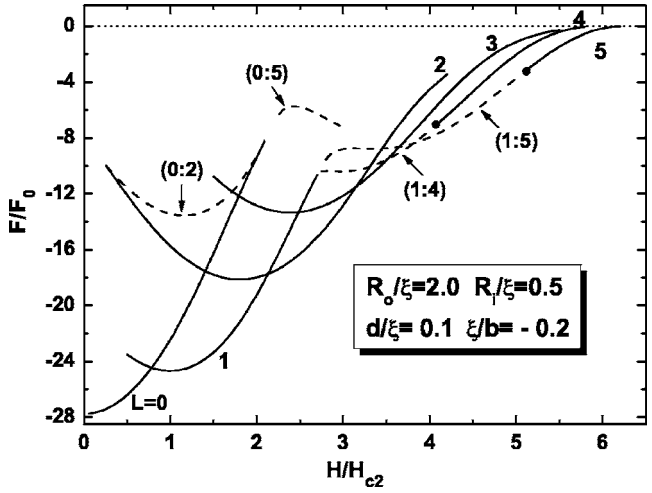

FIG. 12. The free energy as function of the applied magnetic field for a superconducting ring with $R_0/\xi=2.0$, $R_i/\xi=0.5$, $\xi/b=-0.2$, and $d/\xi=0.1$. The different giant vortex states are shown by the solid curves and the multivortex states by the dashed curves. The transitions from the multivortex state to the giant vortex state are indicated by the solid circles.

the CNCR and the region **III** exist. In the case of $R_i>1.75\xi$, $H_{\mathbf{III}}=H_{nuc}$, and only the CNCR exists, i.e., the whole ring is negatively charged as long as the sample is in the superconducting state. The nucleation field H_{nuc} also becomes very large when $R_i\approx R_0$ because of the enhancement of surface conductivity for very small samples. The case given in Fig. 7(b) is for $\xi/b=-0.2$, and that in Fig. 7(c) is for $L=2$. We find that a stronger surface superconductivity effect will depress the regions **I** and **II**. Whereas, for the $L=2$ state, the minimum inner radius needed increases in comparing with the data shown in Fig. 7(a) for the occurrence of region **III** and the CNCR as well as the region **I** disappearance.

Now we study the effect of a ring outer radius on the charge distribution when $\xi/b=-0.1$. At first, Fig. 8 show the nucleation fields H_{nuc} as a function of the outer radius of rings with $R_i/\xi=0.0$ and different ξ/b for the $L=1$ state. We find that the superconducting state can only exist in sufficiently large samples and the region of existence of the superconducting state increases with increasing $|\xi/b|$ values. For $\xi/b=-0.1$, the superconducting state occurs when $R_o/\xi=0.717$, and there are two nucleation fields present, i.e., the upper nucleation field (thin solid curve) and the lower nucleation field (thick solid curve) with increasing outer radius. When $R_o/\xi=1.014$, the lower nucleation field disappears and the superconducting $L=1$ state can exist in a zero magnetic field. As an example, we consider a ring with $R_o/\xi=0.5$ and investigate the charge distribution. Figure 9 shows the phase diagram. The thick solid curve denotes the lower nucleation field (H^1_{nuc}) and the thin solid curve denotes the upper nucleation field (H^2_{nuc}). The solid circle denotes the critical inner radius when the superconducting state can occur. We also can find the region **I**, the region **II**, the CNCR (the region **IV**), and the region **III** seemed very much like those in Fig. 7, but there is no superconducting state of $L=1$ for the small inner radius. When increasing the inner radius, the lower nucleation field (H^1_{nuc}) occurs and decreases to the zero mag-

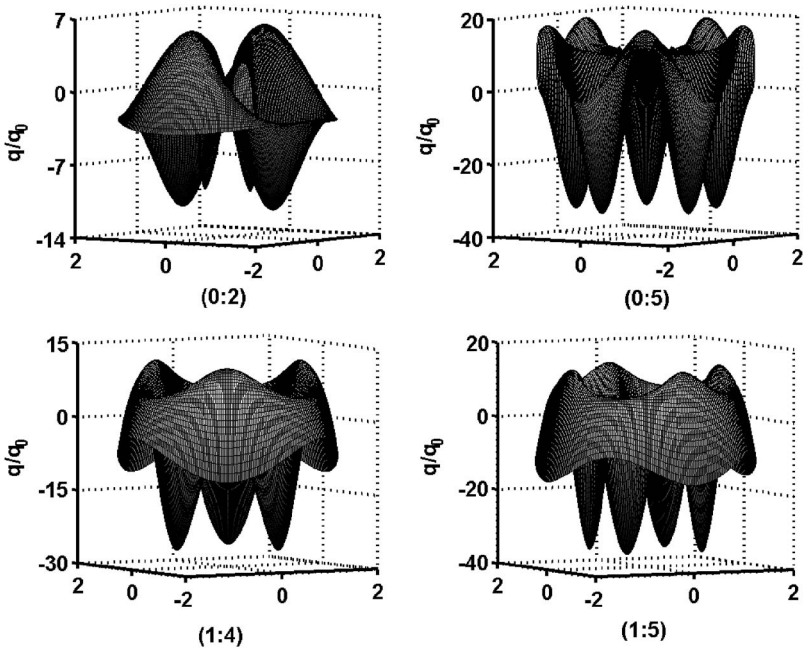

FIG. 13. The charge density distributions for the (0:2) state at the field $H=1.45H_{c2}$, the (0:5) state at the field $H=2.45H_{c2}$, the (1:4) state at the field $H=3.45H_{c2}$, and the (1:5) state at the field $H=4.45H_{c2}$ for a ring with $R_0/\xi=2.0$, $R_i/\xi=0.5$, $\xi/b=-0.2$, and $d/\xi=0.1$.

netic field finally. It is believed that the giant vortex state will not exist in a zero magnetic field when the ring becomes smaller. In addition, we get that the upper nucleation field (H_{nuc}^2) becomes very large compared with larger rings because of the enhancement of surface conductivity for very small samples.

Figure 10 gives the critical inner radii $R_{i,cr}$, $R_{i,cr}^1$, and $R_{i,cr}^2$ dependence of the outer radius R_o for superconducting rings with $\xi/b=-0.1$ and $d/\xi=0.1$ in the $L=1$ state. We find that the $R_{i,cr}$, $R_{i,cr}^1$, and $R_{i,cr}^2$ all increase with increasing the outer radius, and the $R_{i,cr}$ and $R_{i,cr}^1$ reach maximums and then decrease to zero when the outer radius $R_o/\xi=4.468$ and $R_o/\xi=5.056$, respectively. That is to say, the CNCR can also exist in large rings with $R_i/\xi=0$, i.e., disks in the $L=1$ state. In this case, the superconductivity is enhanced with increasing $|\xi/b|$ and the more magnetic field is expelled from the sample and the giant vortex is more compressed in the center. Therefore the superconductor has to induce a larger supercurrent and the negative charge in the sample increases. When the surface enhancement of superconductivity is strong enough, the CNCR will occur. Figure 11 gives the applied magnetic field H-dependence of the radius $\rho*$ for two superconducting disks $R_o/\xi=4.7$ (a), $R_o/\xi=5.2$ (b) in the $L=1$ state, and we can find the CNCR (the region **IV**). For disk (a), because $R_o/\xi=4.7<5.056$, there exist two region **II**. For disk (b), because $R_o/\xi=5.2>5.056$, the $R_{i,cr}^1$ disappears. On the other hand, the region **III** that corresponds to the positive inner charge and negative outer charge also cannot exist in large disks.

IV. VORTEX CHARGE IN THE MULTIVORTEX STATES

For sufficiently large rings the giant vortex state can break up into multivortices.[14–18] The order parameter of the multivortex state in general can be viewed as a superposition of giant vortex states with different L_j

$$\psi(\vec{\rho})=\sum_{L_j=0}^{L} C_{L_j} f_{L_j}(\rho)\exp(iL_j\theta), \tag{20}$$

where L is the value of the effective total angular momentum now which equals the number of vortices in the ring. For the small rings that we studied, we consider states which are built up by only two components in Eq. (20)

$$\psi(\vec{\rho})=C_{L_1} f_{L_1}(\rho)\exp(iL_1\theta)+C_{L_2} f_{L_2}(\rho)\exp(iL_2\theta), \tag{21}$$

where

$$C_{L_1}=\left(\frac{-\Lambda_{L_1}A_{L_2}B_{L_1}+2\Lambda_{L_2}A_{L_1,L_2}B_{L_2}}{A_{L_1}A_{L_2}-4A_{L_1,L_2}^2}\right)^{1/2}, \tag{22}$$

$$C_{L_2}=\left(\frac{-\Lambda_{L_2}A_{L_1}B_{L_2}+2\Lambda_{L_1}A_{L_1,L_2}B_{L_1}}{A_{L_1}A_{L_2}-4A_{L_1,L_2}^2}\right)^{1/2}, \tag{23}$$

$$A_{L_i}=\frac{2\pi d}{V}\int_{R_i}^{R_o}\rho d\rho f_{L_i}^4(\rho), \tag{24}$$

$$A_{L_1,L_2}=\frac{2\pi d}{V}\int_{R_i}^{R_o}\rho d\rho f_{L_1}^2(\rho) f_{L_2}^2(\rho), \tag{25}$$

$$B_{L_i}=\frac{2\pi d}{V}\int_{R_i}^{R_o}\rho d\rho f_{L_i}^2(\rho), \tag{26}$$

and $f_{L_i}(\rho)$ and Λ_{L_i} are determined by Eqs. (16) and (17), respectively.

The energy of the multivortex state becomes[25]

$$F_{L_1,L_2}=\frac{-\Lambda_{L_1}^2A_{L_2}B_{L_1}^2-\Lambda_{L_2}^2A_{L_1}B_{L_2}^2+4\Lambda_{L_1}\Lambda_{L_2}A_{L_1,L_2}B_{L_1}B_{L_2}}{A_{L_1}A_{L_2}-4A_{L_1,L_2}^2}. \tag{27}$$

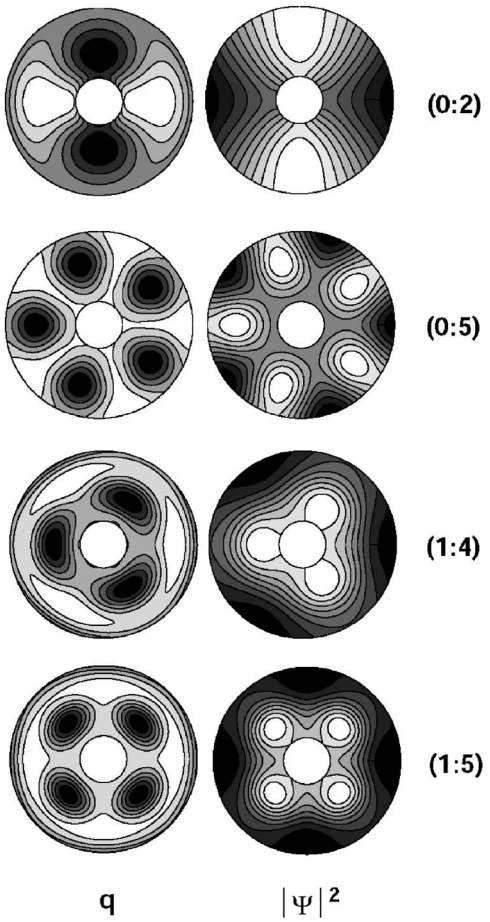

FIG. 14. The contour plots of the charge density distribution and the Cooper pair density distribution for the (0:2) state at the field $H=1.45H_{c2}$, the (0:5) state at the field $H=2.45H_{c2}$, the (1:4) state at the field $H=3.45H_{c2}$, and the (1:5) state at the field $H=4.45H_{c2}$ for a ring with $R_0/\xi=2.0$, $R_i/\xi=0.5$, $\xi/b=-0.2$, and $d/\xi=0.1$.

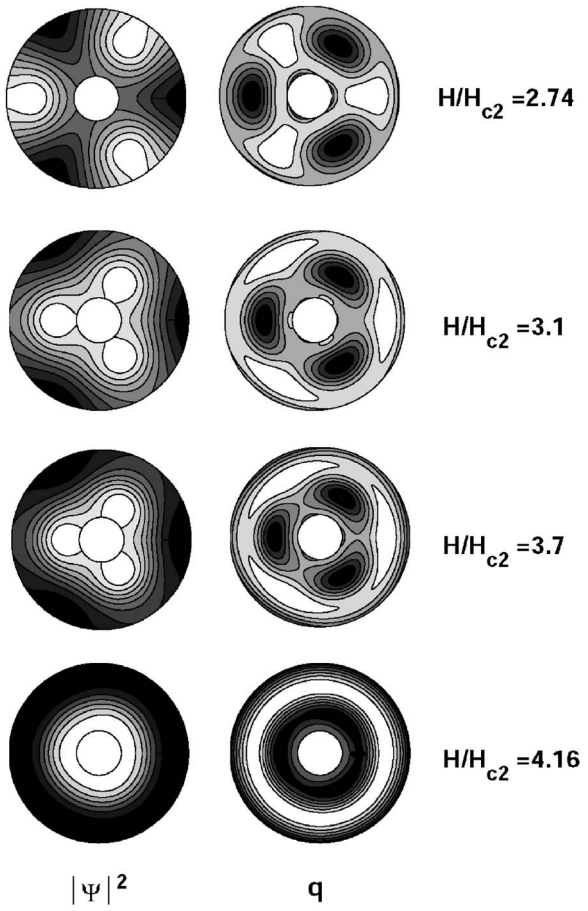

FIG. 15. The contour plots of the Cooper pair density distribution and the charge density distribution for the (1:4) state at the field $H=2.74H_{c2}$, $H=3.1H_{c2}$, $H=3.7H_{c2}$, and $H=4.16H_{c2}$ for a ring with $R_0/\xi=2.0$, $R_i/\xi=0.5$, $\xi/b=-0.2$, and $d/\xi=0.1$.

Earlier analyses have shown[17,25,30] that there exist two kinds of multivortex states: (i) the stable state which corresponds to a minimum of the free energy and (ii) the saddle-point state which correspond to the energy barrier state between states with different vorticity L. In small rings, the confinement effect dominates and only the giant vortex states are stable.[31] But because of the enhanced surface superconductivity, the multivortices will become stable with increasing $|\xi/b|$. As an example, we consider a thin ring with $R_0/\xi=2.0$, $R_i/\xi=0.5$, and $\xi/b=-0.2$. In Fig. 12, the saddle-point state and the stable multivortex state for the ring are given, and we only consider the case of $L\leqslant 5$. We find that there also presents the stable multivortex state in the small ring that we studied because of the enhanced surface superconductivity. We can get that the (0:2) state is a saddle-point state and unstable, and the (0:5) state is only found in the metastable state. When $L\geqslant 4$, the $(1:L)$ states can occur as the metastable state and the ground state (this will not happen in a disk with same outer radius).[25] The charge density distributions over the ring for the (0:2) state at the field $H=1.45H_{c2}$, the (0:5) state at the field $H=2.45H_{c2}$, the (1:4) state at the field $H=3.45H_{c2}$, and the (1:5) state at the field $H=4.45H_{c2}$ are shown in Fig. 13, and their contour plots together with the Cooper pair density are given in Fig. 14. The light regions on the contour plots of the Cooper pair density distribution correspond to low Cooper pair density and the dark regions on the contour plots of the charge density distribution correspond to the region of negative charge location. So we get that the negative charge located around the vortex cores and the positive charge near the edge of the sample. Figure 15 gives the contour plots of the Cooper pair density distribution and the charge density distribution for the (1:4) state at different magnetic fields. With increasing the magnetic field the single vortices in the multivortex state will move towards each other. When $H=3.7H_{c2}$, the (1:4) multivortex state is the ground state and most stable. Further increasing the magnetic field, the transition between the multivortex state and the giant vortex state will take place ($H=4.16H_{c2}$). From the contour plots of the charge density distribution, we can get that the negative charge is pulled towards the inner boundary and the positive charge is pulled towards the outer boundary when the multivortex state becomes more stable with increasing the field. Finally, at the transition field between the multivortex state and the giant vortex state, the negative charge and the positive charge merge together, respectively. We also notice that the negative charge at the outer boundary appears and then increases with increasing the magnetic field.

V. CONCLUSIONS

In conclusion, we study the charge distribution in thin mesoscopic superconducting rings with enhanced surface superconductivity by using the phenomenological Ginzburg-Landau theory. We find that the surface enhancement of the superconductivity effect can increase the negative charge of the sample. A complete negative charge distribution, besides conventional distributions, in the Meissner and the giant vortex states is found. In the Meissner state for a ring with a small inner radius we also find one type charge distribution that can only be found in the giant vortex state before there is any enhanced surface superconductivity. For a different inner radii and outer radii, different types charge distributions present. When fixing the outer radius the critical inner radii of different states occurring just needs to be smaller for larger $|\xi/b|$ values. We also investigated the effect of rings outer radius on the charge distributions and find that the upper nucleation field and the lower nucleation field present in rings with smaller outer radius as well as the complete negative charge distribution which can exist in disks with a larger radius. As for the $L>1$ state, for example $L=2$ state, we also find the similar charge distributions which occur in the $L=1$ state, but a larger critical inner radius is needed. For the charge distribution in a multivortex state, we find that the surface enhancement of superconductivity can stabilize the multivortex state as the ground state (i.e., with minimal energy) in mesoscopic superconducting rings and the stable multivortex state is found in small rings with the enhanced surface superconductivity that we studied. The charge density $q(x,y)$ distributions as well as the contour plots of the charge density distribution and the Cooper pair density distribution of different multivortex states are given. We find that the negative charge located around the vortex cores and positive charge are near the edge of the sample. When a multivortex state becomes more stable, the negative charge and the positive charge are pulled towards the inner boundary and the outer boundary of the sample, respectively.

Finally, we discuss briefly the feasibility of the experimental observations of the charging effect. The detection of the vortex charge in type-II superconductors by scanning tunneling microscopy has been discussed by Blatter *et al.*[2] The vortex charge in the high-temperature superconductor (HTSC) $YBa_2Cu_3O_7$ was detected by the nuclear magnetic resonance method.[3] It has been shown that the vortex charge due to the opening of the energy gap or the transition to superconducting is of the order[1] $\Delta/E_F - [(m/2\hbar^2)\pi^2\Delta\xi^2]^{-1}$. [We have used the expression: $E_F=(m/2\hbar^2)\pi^2\Delta^2\xi^2$, for a metallic superconductor in the clean limit (cf. Ref. 11).] This ratio for type-I metallic superconductors is then orders smaller than that of HTSC, for which the vortex charge is of the order of 10^{-3} e when $\xi_0=5$ Å.[1] Consequently, the above mentioned techniques could be challenged because of limited accuracy. Recently, Geim *et al.*[32,33] developed the ballistic Hall magnetometry, and vortex charge associated with abnormalities in mesoscopic disks of the metallic superconductor (aluminum) have been signaled by using this technique,[34] which sheds lights on experimental detection on the vortex charge in mesoscopic metallic superconductors. In addition, this technique will be useful to detect the vortex charge in type-II metallic superconductors, e.g., the niobium-alloy material, Nb_3Sn, where the coherence length is ~ 4 nm, and the critical temperature $T_c=18$ K, or $\Delta(0)\sim 4$ meV,[35] from which a value of Δ/E_F is estimated in the order of 3.5×10^{-2} that is comparable to the value of 10^{-1} for the typical HTSCs.

ACKNOWLEDGMENTS

This work is supported by the National Natural Science Foundation of China (Grant No. 60371033) and by the Shanghai Leading Academic Discipline Program, China.

[1] D. I. Khomskii and A. Freimuth, Phys. Rev. Lett. **75**, 1384 (1995).
[2] G. Blatter, M. Feigel'man, V. Geshkenbein, A. Larkin, and A. van Otterlo, Phys. Rev. Lett. **77**, 566 (1996).
[3] K. I. Kumagai, K. Nozaki, and Y. Matsuda, Phys. Rev. B **63**, 144502 (2001).
[4] P. Lipavsky, J. Kolacek, K. Morawetz, and E. H. Brandt, Phys. Rev. B **66**, 134525 (2002).
[5] Y. Chen, Z. D. Wang, J. X. Zhu, and C. S. Ting, Phys. Rev. Lett. **89**, 217001 (2002).
[6] M. Machida and T. Koyama, Phys. Rev. Lett. **90**, 077003 (2003).
[7] N. Hayashi, T. Isoshima, M. Ichioka, and K. Machida, Phys. Rev. Lett. **80**, 2921 (1998).
[8] E. Simanek, Phys. Rev. B **65**, 184524 (2002).
[9] S. V. Yampolskii, B. J. Baelus, F. M. Peeters, and J. Kolacek, Phys. Rev. B **64**, 144511 (2001).
[10] B. H. Zhu, S. P. Zhou, G. Q. Zha, and K. Yang, Phys. Lett. A **338**, 420 (2005).
[11] P. G. de Gennes, *Superconductivity of Metals and Alloys* (Addison-Wesley, New York, 1994).
[12] P. G. de Gennes and J. Matricon, Rev. Mod. Phys. **36**, 45 (1964).
[13] W. V. Pogosov, A. L. Rakhmanov, and E. A. Shapoval, Physica C **356**, 225 (2002).
[14] J. J. Palacios, Physica B **256**, 610 (1998).
[15] J. J. Palacios, Phys. Rev. Lett. **84**, 1796 (2000).
[16] J. J. Palacios, Phys. Rev. B **58**, R5948 (1998).
[17] V. A. Schweigert and F. M. Peeters, Phys. Rev. Lett. **83**, 2409 (1999).
[18] V. A. Schweigert, F. M. Peeters, and P. S. Deo, Phys. Rev. Lett. **81**, 2783 (1998).
[19] V. A. Schweigert and F. M. Peeters, Phys. Rev. B **57**, 13817 (1998).
[20] V. V. Moshchalkov, X. G. Qiu, and V. Bruyndoncx, Phys. Rev. B **55**, 11793 (1997).
[21] A. K. Geim, S. V. Dubonos, J. J. Palacios, I. V. Grigorieva, M. Henini, and J. J. Schermer, Phys. Rev. Lett. **85**, 1528 (2000).
[22] G. F. Zharkov, V. G. Zharkov, and A. Yu. Zvetkov, Phys. Rev. B **61**, 12293 (2000).

[23] G. F. Zharkov, Phys. Rev. B **63**, 224513 (2001).
[24] W. V. Pogosov, Phys. Rev. B **65**, 224511 (2002).
[25] S. V. Yampolskii and F. M. Peeters, Phys. Rev. B **62**, 9663 (2000).
[26] B. J. Baelus, S. V. Yampolskii, F. M. Peeters, E. Montevecchi, and J. O. Indekeu, Phys. Rev. B **65**, 024510 (2002).
[27] J. Kolacek, P. Lipavsky, and E. H. Brandt, Phys. Rev. Lett. **86**, 312 (2001).
[28] E. Jakeman and E. R. Pike, Proc. Phys. Soc. London **91**, 422 (1967).
[29] M. Machida and T. Koyama, Physica C **378**, 443 (2002).
[30] B. J. Baelus, F. M. Peeters, and V. A. Schweigert, Phys. Rev. B **63**, 144517 (2001).
[31] B. J. Baelus, F. M. Peeters, and V. A. Schweigert, Phys. Rev. B **61**, 9734 (2000).
[32] A. K. Geim, J. G. S. Lok, S. V. Dubonos, J. C. Maan, L. Theil Hansen, and P. E. Lindelof, Appl. Phys. Lett. **71**, 2379 (1997).
[33] A. K. Geim, I. V. Grigorieva, S. V. Dubonos, J. G. S. Lok, J. C. Maan, A. E. Filippov, and F. M. Peeters, Nature (London) **390**, 259 (1997).
[34] A. K. Geim, S. V. Dubonos, I. V. Grigorieva, K. S. Novoselov, F. M. Peeters, and V. A. Schweigert, Nature (London) **407**, 55 (2000).
[35] V. Guritanu, W. Goldacker, F. Bouquet, Y. Wang, R. Lortz, G. Goll, and A. Junod, Phys. Rev. B **70**, 184526 (2004).